NTU Journal for Renewable Energy (2024) Vol. 7 (1): 34 - 45
DOI: https://doi.org/10.56286/ntujre.v7i1

IRAQI Academic Scientific Journals

EISSN: 2788-9920
NTU Journal for Renewable Energy
Available online at:
https://journals.ntu.edu.iq/index.php/NTU-JRE

# Experimental Investigation in Cross-Flow Heat Transfer of Air Over *LFFTBHE*

**Ahmed H. Ahmed[a,b,*], Maki H. Zaidan[a], Manar S.M. Al-Jethelah[a]**

[a]Tikrit University /Department of Mechanical Engineering/College of Engineering /Tikrit/ Iraq

[b]Northern Technical University/ Hawija Technical Institute/ Renewable Energy Research Unit

**Article Information**

Received: 02 – 06 - 2024
Accepted: 22 – 07 - 2024
Published: 07 – 09 - 2024

**Corresponding Author:**
Ahmed H. Ahmed

**Email:**
ahmedhasan_hwj@ntu.edu.iq

**Keywords:**
Forced convection, *LFFTBHE*, Staggered flat tube, Upstream fin length.

**ABSTRACT**

The heat transfer and fluid flow of airflow in a staggered flat tube bank in crossflow with laminar forced convection are experimentally investigated and presented in this study. Two rows of finned tubes were placed perpendicular to the flow direction. The air velocity varies between 0.29 m/s–1.46 m/s, and the Reynolds number approximately ranged from $223 \leq Re \leq 1114$. The surface temperature in all tubes is constant. The dimensionless upstream fin length ($L_u/D_T$=0.4, 0.6, 0.8, and 1), respectively, and the dimensionless downstream fin length( $L_d/D_T)of$ 0.8, the dimensionless transverse pitch ($S_T/D_T$) of 3.0, the dimensionless longitudinal pitch ($S_L/D_T$) =4.0, and the dimensionless fin angle ($\theta ds$)=0.52 with constant physical properties. The results show that the Nusselt number, friction factor, and Colburn factor are inversely proportional to the upstream fin length. The percentage of deficient was 14%, 12%, and 35%, respectively, in contrast to the Bejan number, where the percentage of improvement was 11%. Correspond to the highest value of the Reynolds number. This is fully consistent with the principles of Constructal Law.

## 1. Introduction

A number of crucial industrial processes are idealized by the heat transfer ($HT$) and fluid flow ($FF$) in tube bundles. Crossflow heat exchangers ($CFHE$) openly use tube banks since the design still depends on empirical correlations between $HT$ and pressure drop ($PD$).

In many chemical and thermal engineering processes, heat exchangers ($HE_s$) with tube bundles in crossflow are of great operational importance [1–7]. Heat exchanger efficiency improvements would subsequently result in material, space, and cost reductions.

The $PD$ and $HT$ between a fluid flow and the heat exchanger must be understood beforehand to design a heat exchanger, determine ideal parameters, and specify operating performance criteria [8,9].

The properties of $HE$ have been investigated by experimental and mathematically based numerical simulations and empirical observations [10–14]. Even though they haven't been evaluated as much, flat tubes are important in many technological applications, such as car radiators and contemporary heat exchangers. Recently, designs for automobile evaporators and condensers used in air conditioning systems have been made available. The cost of building flat tube heat exchangers has become more favourable due to recent advancements in automotive aluminium fabrication technology [15,16].

The study examined the average and local heat transfer coefficients for circular tube bundle problems over a broad range of Reynolds numbers and transverse and longitudinal pitches [17]. Moreover, experimental studies have shown that computational fluid dynamics is a reasonably priced alternative that may optimize the $HE$ design and provide a fast, accurate solution [18–20]. Flat or flattened tubes are essential parts of many technological applications, such as contemporary car radiators and $HE_s$. Flat tubes have not been analyzed often, even though several researchers have researched heat transfer and fluid flow over objects of diverse forms. Recently, condensers and evaporators for car air conditioning have been using flat tubes. Advancements in automobile-brazed aluminium production techniques have resulted in a decrease in their cost [21–23]. A wide variety of longitudinal and transverse pitches, Reynolds numbers, and flat tube shapes have been studied numerically in relation to the local and average heat transfer coefficients for the tube array [24–26].

An analysis using numerical methods to examine the impact of oval tubes' aspect ratio on the properties of pressure drop and heat transfer from the air side of a finned-tube $HE$. The identical circumferences of circular and elliptical (flat and oval) tube designs were compared by the authors. The tube's hydraulic diameter determines the Reynolds numbers, which vary from 297 to 999 for the low airflow velocities of 1, 2, and 3 m/s. According to the research, the $PD$ in the air-side (external flow) grows as the aspect ratio of a tube ((1/e) e is eccentricity) increases, while the $PD$ in the interior tube conducted increases as well [27]. The experimental study of airflow and $HT$ over a staggered flat tube bundle was conducted by Ishak et al. [28]. Based on a hydraulic diameter range of 373 to 623 and a heat flux of 967.9–3629.70 $W/m2$ delivered to the tube's outer surface,

the Reynolds number range is determined. The $PD$ and heat transfer coefficient were discovered by the author to rise as the Reynolds number rose. However, the research also looked at the relationship between heat transmission and Reynolds number. These investigations revealed that both numerical and experimental research had been done on a variety of tube shapes, including cylindrical, elliptic, and others. Numerical research had also been done on both in-line and staggered flat tube arrangements, and experimental research had also been done on an in-line flat tube bank. Thus, the primary goal of this work is to investigate the pressure drop and heat transfer across a longitudinal fin flat tube bank that is staggered. The Reynolds numbers vary from 223 to 1114 when the surface temperature is constant. The thermal and hydraulic performance of four dimensionless upstream fin lengths, 4.0, 6.0, 8.0, and 1, was examined.

## 1. Experimental Setup and Details:

A wind tunnel specifically designed and built for forced convection heat transfer purposes was used for the experimental study. The tests were conducted in the manufacturing of a Cross flow heat exchanger put in a low-speed wind tunnel to evaluate heat transfer and pressure losses at the laboratories of the Renewable Energy Research Unit, Hawija Technical Institute. One component of the experimental equipment is a low-speed wind tunnel. A galvanized steel low-speed open-circuit wind tunnel was constructed to enable thorough research into the operation and principles of heat exchangers. The device consists of six main sections: an exhaust air section with a variable slide valve to control airflow, an extended region, a reduction unit, a normal unit, a test section, and an AC-powered suction fan. In the test section, a Pitot tube is used to measure the static pressure differential across the rods. An anemometer can be used to measure air velocity at any vertical position within the working part.

It also has three power supplies: one for managing the speed of the $AC$ motor and two for adjusting the heat source of the cartilage heaters implanted into the flat tube element. Before the test section, a 400 mm-long normal unit was placed to give the flow time to develop before the fin arrangement arrived fully. To regulate the flow before entering the test portion, metal screens were placed at the entrance of the standard unit. Within the wind tunnel, an exhaust fan was installed and directly powered by an electric motor (Model EPMB 4E 250 single phase, 230 V, 0.75 HP, and 50 Hz). Figure 1 shows the schematic representations of the wind tunnel used in this experimental inquiry. Figure 2 shows the velocity profile at the empty case and the wind tunnel calibration of the enlarged region. Figure 3 describes the calibration of the thermocouple. In the test rig, thirty-two thermocouples were utilized to measure the temperature variation caused by forced convection. Two thermocouples were positioned at the test rig's layout inlet Tin and throughout its width. Four thermocouples at two different tube surfaces ($T_{s,1}-T_{s,4}$).). As indicated by the schematic representations of the thermocouple installations, there are four thermocouples at the outlet airflow ($T_{out,1}-T_{out,4}$) and three thermocouples in the fin surface with two locations. Figure 4. Four thermocouples at various places on the exterior test section surfaces ($T_{os,1}-T_{os,4}$) were used to estimate the heat losses. $T_O$ Measure the free stream temperature, a second thermocouple ($T_{air}$) was positioned $150\ mm$ in front of the test module on the enlarged area.

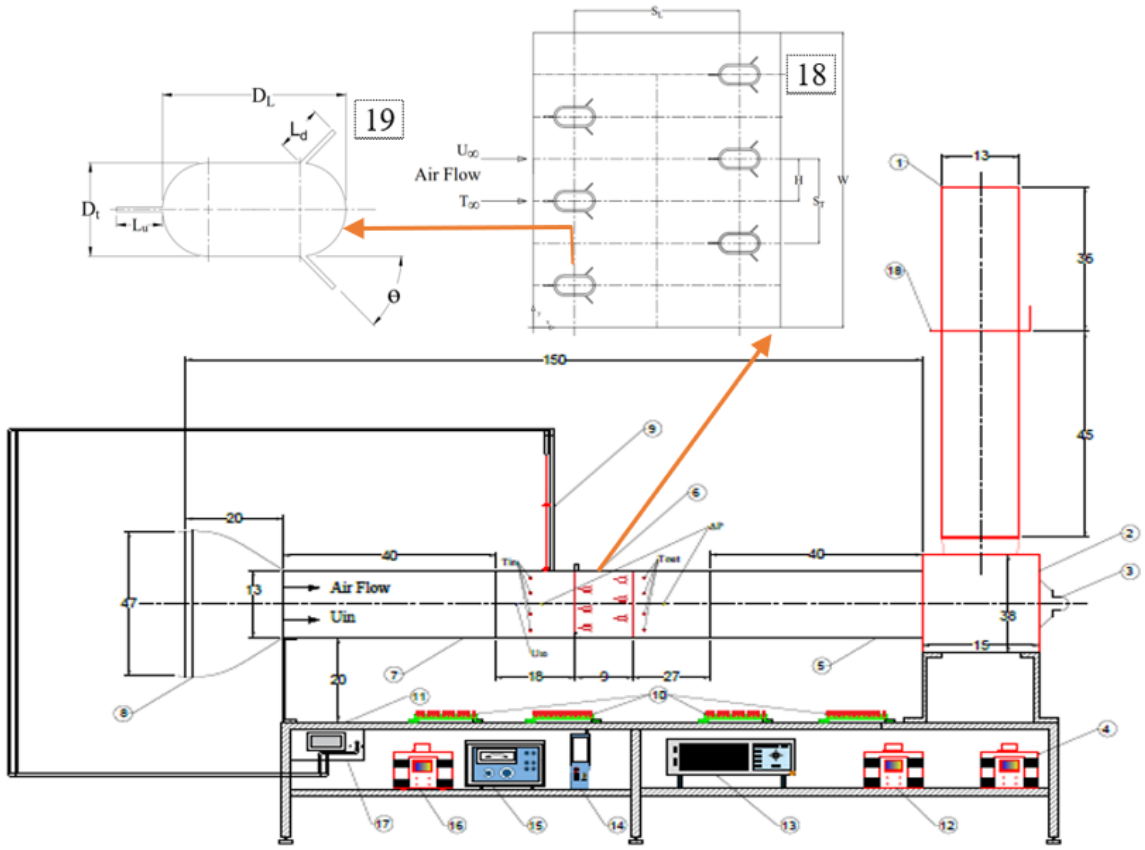


**Figure 1.** Schematic display of the experimental approach with all dimensions in mm.

1- Exhaust air section
2- Suction fan
3- A.C motor
4- Controller
5- Extended region
6- Test section
7- Normal unit
8- Reduction unit
9- Pitot tube
10- Pass board
11- Base frame with Stand plate
12- A-C Power supplies the first raw
13- Data logger
14- Hot wire anemometer
15- D-C power supply
16- A-C power supply second raw
17- Petot tube monitor
18- Rows of LFFTB in crossflow
19- Front view of longitudinal fin tube

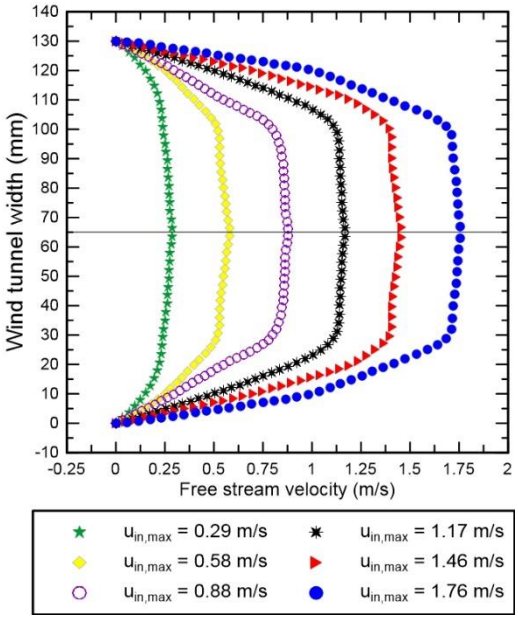


**Figure 2.** Free stream velocity profile in low-speed wind–tunnel.

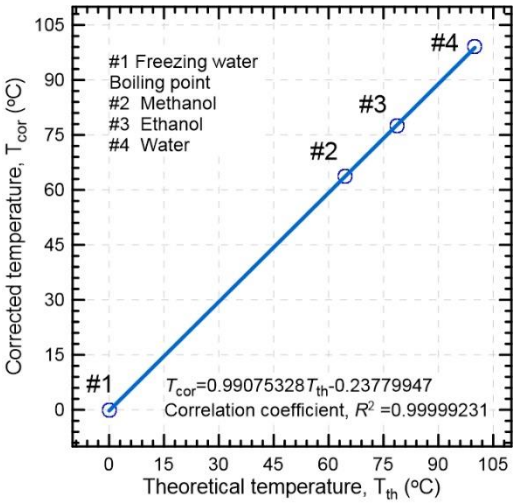


**Figure 3.** A typical thermocouples curve fitting.

## 2. Data Collection

This experiment includes laminar external airflow. The following computations rely on the following relations for the necessary air characteristics [29]:

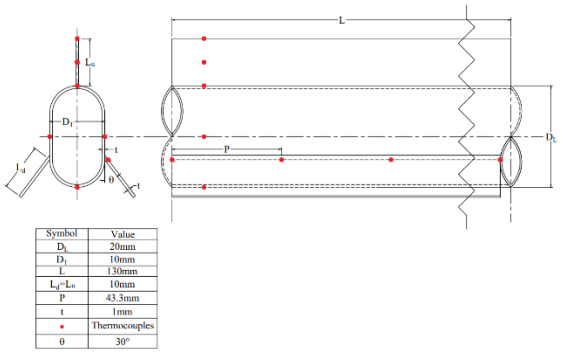

| Symbol | Value |
|---|---|
| $D_h$ | 20mm |
| $D_1$ | 10mm |
| L | 130mm |
| $L_d$=$L_m$ | 10mm |
| P | 43.3mm |
| t | 1mm |
| • | Thermocouples |
| θ | 30° |

**Figure 4.** The schematic representations of the thermocouple's installations.

$$\rho_a = [1E-05T^2 - 0.0044Tb + 1.2868], \frac{\text{kg}}{\text{m}^3} \quad (1)$$

$$c_{Pa} = [-2E-07Tb^4 + 5E-05Tb^3 - 004Tb^2 + 0.1354Tb + 1005.4], \frac{J}{(kg\ K)} \quad (2)$$

$$k_a = [-2E-08Tb^2 + 8E-05Tb + 0.0236], \quad \frac{\text{W}}{(\text{m K})} \quad (3)$$

$$\mu_a = [-23E-11Tb^2 + 5E-08Tb + 2E-05], \quad \frac{\text{kg}}{(\text{m s})} \quad (4)$$

$$\alpha_a = [2E-10Tb^2 + 1E-07Tb + 2E-05], \quad \frac{\text{m}^2}{\text{s}} \quad (5)$$

$$v_a = [1E-10Tb^2 + 9E-08Tb + 1E-05], \quad \frac{\text{m}^2}{\text{s}} \quad (6)$$

$$Pr_a = [5E-07Tb^2 - 0.0003Tb + 0.7372], \quad (7)$$

Where Air properties correlations $(298\text{K}) \leq Tb \leq 373(\text{K})$. The dimensionless heat transfer rate is expressed as [30]:

$$\hat{Q} = \frac{Q_{\text{in}}}{W_x \times H_y \times L} \times \frac{\left(D_{\text{h,o}}\right)^2}{k_a\left(\overline{T_w} - \overline{T_{\text{in}}}\right)} \qquad (8)$$

Where $D_{\text{h, o}}$is the outside hydraulic diameter, $Wx$ array length, $Hy$ array height, and $L$ is the array width can be assumed to be 1 for 2-dimension analyses. The inlet air temperature is $25\ °C$. The following equation can be used to obtain the outer side hydraulic diameter of the flattened tube:

The heat input is divided by the restriction volume $(Wx \times Hy \times L)$, the thermal conductivity of the fluid, and the hydraulic diameter of the flat tube.

$$d_h = \frac{4A}{P} \qquad (9)$$

The first law of thermodynamics can be applied to an elementary channel, i.e., via energy balance in a channel. The input heat gain in all elemental can be described as follows:

$$Q_{\text{in}} = \dot{m}_{\text{a}}\, c_{P_a}\left(\overline{T}_{\text{out}} - \overline{T}_{\text{in}}\right) \qquad (10)$$

Where $\dot{m}_{\text{a}}$ is the overall air mass flow rate $(kg/s)$ input in the tube bundle heat exchanger?

The channel element is based on the sum of all computational domain units in the $z-axis$. Thus, the defined elementary air mass flow rate can be written as follows:

$$\dot{m}_{\text{a}} = \rho_{\text{a}}\, u_{\text{in}}(W\text{x} \times H\text{y}) \qquad (11)$$

The average convection coefficient, which is defined as:

$$\bar{h} = \frac{q_{\text{air}}}{A_{\text{s}}\left[\overline{T_{\text{s}}} - \left(\frac{\overline{T_{\text{in}}} + \overline{T_{\text{out}}}}{2}\right)\right]} \qquad (12)$$

It is usually used in the overall Nusselt number, which is defined as:

$$Nu = d_h \times \frac{\bar{h}}{k_{\text{f}}} \qquad (13)$$

Where $K_f$, is the thermal conductivity of air. The Reynolds number based on the fin length is defined as:

$$R_e = U_\infty \times d_h \times (\rho_a/\mu_a) \qquad (14)$$

Where, $U_\infty$ Is the air-free stream velocity and dh is the hydraulic diameter [31]:

The pressure drop is expressed as:

$$\Delta P = P_{in} - P_{\ out} \qquad (15)$$

Colburn factor $j$ is calculated by [32]:

$$j = \frac{Nu}{Re * Pr^{1/3}} \qquad (16)$$

Friction factor ƒ is defined as [32]:

$$\text{ƒ} = \frac{\Delta P \times d_h}{2 \times \rho \times L \times U_\infty^2} \qquad (17)$$

Thermal hydraulic performance $\text{h}_f$ It is defined as [32]:

$$h_f = \frac{j}{f} \qquad (18)$$

The dimensionless pressure drop is expressed as:

$$\hat{P} = \frac{2 \times \Delta P}{\rho \times U_\infty^2} \qquad (19)$$

The independent parameters (such as temperature, dimensions, etc.) were found, including aligned (B) and accuracy errors (P), using the collect square root (RSS) method[33, 34].

$$B = \left[B_1^2 + B_2^2 + B_3^2 + ... + B_n^2\right]^{1/2}; \quad P = \left[P_1^2 + P_2^2 + P_3^2 + ... + P_n^2\right]^{1/2} \tag{20}$$

Elemental errors were integrated to obtain 95% for confidence uncertainty (U) using the following relationship:

$$U = \left[B^2 + P^2\right]^{1/2} \tag{21}$$

$$B = \pm\left[\left(\frac{1}{2}\text{Resolution}\right)^2 + (\text{Accuracy})^2\right]^{1/2} \tag{22}$$

The uncertainties of parameters can be estimated in terms of absolute values (%) as in table 1.

## 3. Results and discussion

The optimum of the staggered $LFFTBHE$ at a fixed volume was considered concerning the upstream fin length variable, and the other parameters are constant. The dimensions of the fixed volume optimum procedure are presented in Figure 5. The experimental study for the laminar forced convection heat transfer across $LFFTBHE$ is presented in this section and is based on the constructal design method with staggered arrays. When $Re_{dh}$ and other specifications are tabulated in Figure 5. Figures 6 and 7 represent the relationship between the Nusselt number concerning upstream fin length and Reynolds numbers, respectively. The geometric parameter in the arrangement is the upstream fin length. It is clear from the figure above that the Nusselt number is inversely proportional to the upstream fin length, unlike the Reynolds number and the percentage of deficient was 14%.

The main reason for this phenomenon is the separation of the fluid in the first stages, which prevents it from colliding with the upstream fin. The adjacent layer grows due to the absence of the effect of fluid momentum does not allow it to sweep the adjacent layer. This process is accompanied by an increase in thermal insulation between the surface of the pipe and the fluid, and as a result, the heat transfer between the fluid and the surface decreases, and the Nusselt number decreases, considering that it is a function of the heat transfer coefficient by forced convection with the hydraulic diameter constant. Figures 8 and 9 represent the relationship between the Bejan number to upstream fin length and Reynolds numbers respectively. It is clear from the figure above that the Bejan number is proportional to the upstream fin length, as well as the Reynolds number, and the percentage of improvement was 11%.

The process of the fluid colliding with the front of the fin almost completely cancels the momentum resulting from the collision, or rather, it disappears relatively as the upstream fin length increases. The fluid tends to fill the space between the tubes, so friction begins to decrease relatively, accompanied by a clear decrease in the pressure drop, and thus the pumping power decreases. This process is accompanied by an increase in the speed of the fluid displaced between the rows of the heat exchanger to collide with the rear fins. Therefore, the resulting Bejan number gained can be considered as a result of this procedure. Figures 10 and 11 represent the relationship between the friction factor for upstream fin length and Reynolds number, respectively. It is clear from the figure above that the friction factor is inversely proportional to the upstream fin length and the Reynolds number and the percentage of deficient was 35%.

The above figure refers to the friction resulting from the movement of the fluid, so, logically, any increase in the Reynolds number is accompanied by an increase in friction, except for the Colburn factor, the hydraulic, and thermal performance factor, as the effect is joint of the heat transfer and momentum come from fluid flow, and this

explains the difference with the friction factor. The results show that the Colburn factor is inversely proportional to the upstream fin length, and the percentage of deficient was 12%. This is a sufficient explanation for figures 12 and 13.

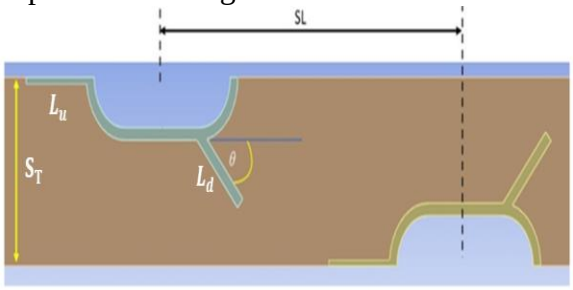


**Figure 5.** Geometric parameters of $LFFTBHE$ arrangements with up-stream fin length variable.

| No. | Parameters | Scale | Unit |
|---|---|---|---|
| 1 | $S_T$ | 30 | mm |
| 2 | $S_L$ | 40 | mm |
| 3 | $Lu$ | Variable | mm |
| 4 | $T_s$ | 90 | ℃ |
| 5 | $Ld$ | 8 | mm |
| 6 | $\theta$ | 30° | Degree |
| 7 | $Re$ | $223 \leq Re \leq 1114$ | |
| 8 | $T_\infty$ | 25 | ℃ |

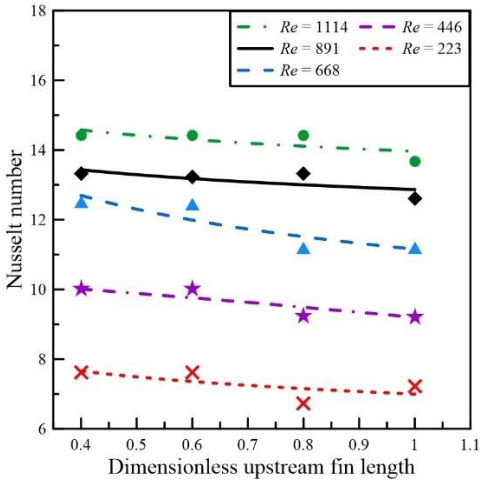


**Figure 6.** Influence of Nusselt number on dimensionless upstream fin length for various Reynolds numbers.

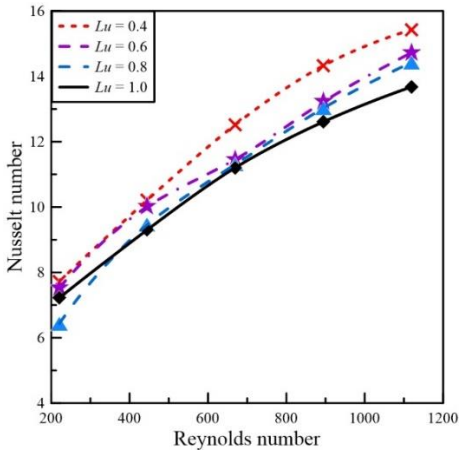


**Figure 7.** Variation of Nu number on Re numbers for various dimensionless upstream fin length.

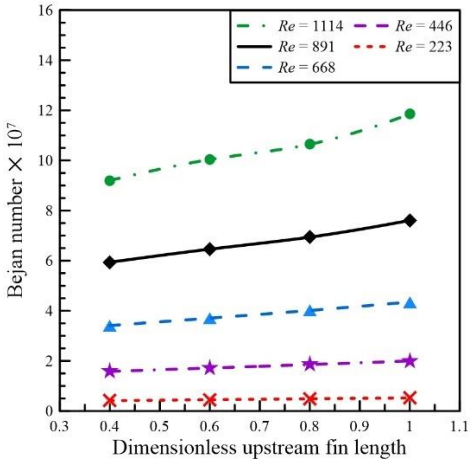


**Figure 8.** Influence of Began number on upstream fin length for various Re numbers.

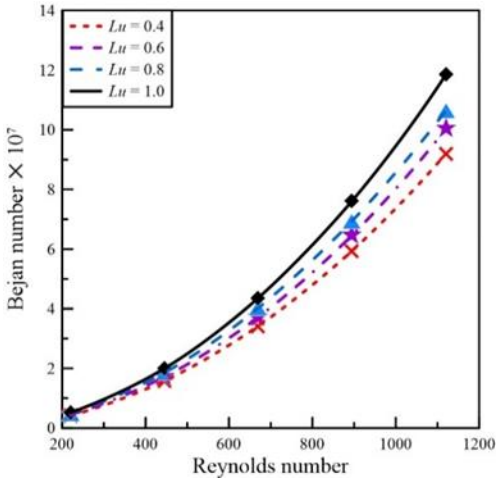


**Figure 9.** Influence of Began number on Reynolds numbers for various dimensionless upstream fin lengths.

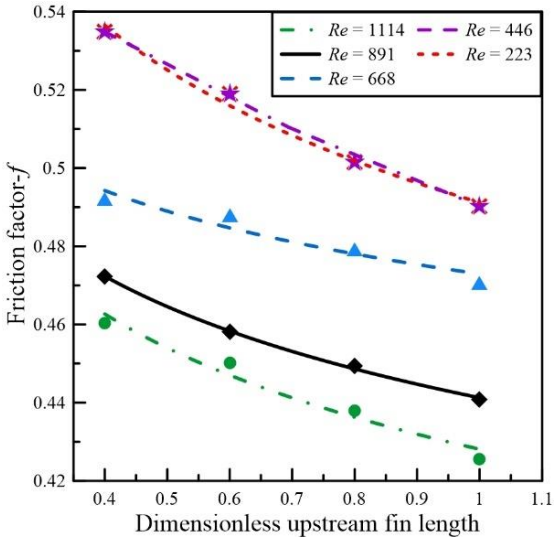


**Figure 10.** Dimensionless friction factor against dimensionless upstream fin length for various Reynolds numbers.

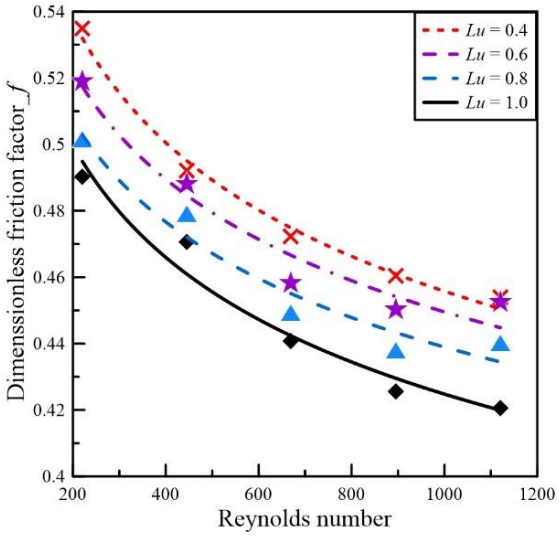


**Figure 11.** Dimensionless friction factor against Reynolds numbers for various dimensionless upstream fin lengths.

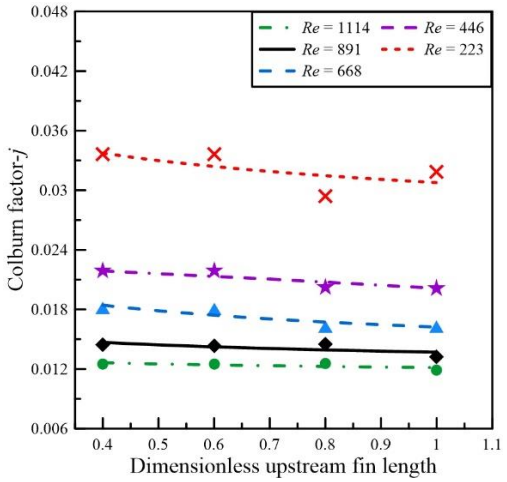


**Figure 12.** Dimensionless Colburn factor against dimensionless upstream fin length for various Reynolds numbers.

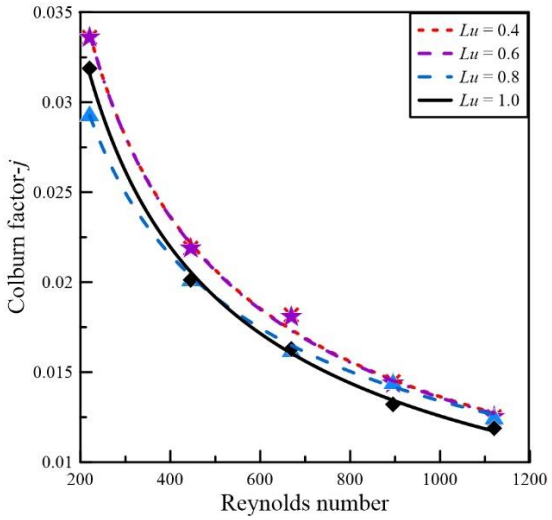


**Figure 13.** Dimensionless Colburn factor against Reynolds numbers for various dimensionless upstream fin lengths.

## 4. Conclusion

The construction of a two-dimensional experimental model of the $LFFTBHE$ has been completed successfully utilizing the constructal design approach. Given that the results obtained showed the behaviour of the heat transfer and flow fields as a function of the variation of the dimensionless upstream fin length for $0.4 \leq Lu/DT \leq 1$ and $223 \leq Re \leq 1114$ flow fields. Optimal heat transfer is achieved for the examined operating

circumstances and heat exchanger geometry with minimal pressure drop. When the dimensionless $Lu/DT = 4$, more heat is transferred (high Nusselt number). The pressure drop is decreased (law Bejan number), and the Reynolds numbers are increased for dimensionless $Lu/DT < 4$. The Began number increases if upstream fin length increases for any Reynolds. As Reynolds numbers rise, the isothermal floods diminish. The flow recirculation region grows as the Reynolds number rises. As the Reynolds number increases, so does the average Nusselt number of airflows. Lastly, as the upstream fin length increases, the average Nusselt number drops. The friction factor and Colburn factor are inversely proportional to the upstream fin length and the Reynolds number.

## Acknowledgements

The authors thank the Faculty of Mechanical Engineering at Tikrit University and Northern Technical University, Technical Institute, Renewable Energy Research Unit, Hawija, Iraq.

## References

[1] A. Žukauskas: Adv. Heat Trans. Vol. 8 (1972), p. 93.

[2] C. Liang and G. Papadakis: J. Fluid Struct. Vol. 23 (2007) p.1215.

[3] E. Buyruk, M.W. Johnson and I. Owen: Int. J. Heat Fluid Fl. Vol.19 (1998), p. 223.

[4] F.P. Incropera, D.P. Dewitt, T.L. Bergman and A.S. Lavine: Fundamentals of Heat and Mass Transfer, 6th ed. (John Wiley & Sons Inc., New York 2007).

[5]V.K. Mandhani, R.P. Chhabra &V. Eswaran: Chem. Eng. Sci. Vol. 57(2002)p. 379.

[6] Y. Kaptan, E Buyruk and A. Ecder: Int. Commu. Heat Mass. Vol. 35 (2008), p. 1153.

[7] Y.Q. Wang, L.A. Penner and S.J. Ormiston: Numer. Heat Tr., Part A Vol. 38 (2000), p. 319.

[8] Ahmed, A.H., M.H. Zaidan, and M.S. Al-Jethelah, Aheat transfer and fluid flow characteristics in a TBHE based on constructal design: An overview. NTU Journal of Renewable Energy, 2023. 4(1): p. 57-96.

[9] Al-Jewaree, H., An experimentally investigate the fin thermal performance to the different fin spaces by natural convections. Al-Kitab Journal for Pure Sciences, 2018. 2(1).

[10] Žukauskas A. Heat transfer from tubes in crossflow, in Advances in Heat Transfer. Elsevier. 1972; 8:93-160.

[11] Siddiqui FA, Dasgupta ES, Fartaj A. Experimental investigation of air side heat transfer and fluid flow performances of multi-port serpentine crossflow mischannel heat exchanger. Int J Heat Fluid Flow. 2012;33(1):207-219.

[12] Tahseen TA, Ishak M, Rahman M. A numerical study laminar forced convection of air for in-line bundle of cylinders crossflow. Asian J Scientific Res. 2013;6(2):217-226.

[13] Zhang L-Z, Zhong W-C, Chen J-M, Zhou J-R. Fluid flow and heat transfer in plate-fin and tube heat exchangers in a transitional flow regime. Numerical Heat Transfer, Part A: Appl. 2011;60(9):766-784.

[14] Matos R, Laursen TA, Vargas JVC, Bejan A. Three-dimensional optimization of staggered finned circular and elliptic tubes in forced convection. Int J Therm Sci. 2004;43(5):477-487.

[15] Suryanarayana, K.V., Srinivasa Rao, G., Reddy Prasad, D.M., Sharma, K.V. and Sarma, P.K. 2011. Experimental analysis of heat and mass transfer in a packed bed. Journal of Mechanical Engineering and Sciences, 1: 124-132.

[16] Webb, R. L. and Kim, N. H. 1994. Principl of enhanced heat transfer. 2nd ed. New York: John Wiley and Sons.

[17] Han H, He Y-L, Li Y-S, Wang Y. A numerical study on compact enhanced fin-and-tube heat exchangers with oval and circular tube configurations. Int J Heat Mass Transfer. 2013;65:686-695.
[18] Khan WA, Culham RJ, Yovanovich MM. Analytical model for convection heat transfer from tube banks. J Thermophys Heat Transfer. 2006;20(4):720-727.
[19] Bhutta MMA, Hayat N, Bashir MH, Khan AR, Ahmad KN, Khan S. CFD applications in various heat exchangers design: a review. Appl Therm Eng. 2012;32:1-12.
[20] Ibrahim TK, Basrawi F, Mohammed MN, Ibrahim H. Effect of perforation area on temperature distribution of the rectangular fins under natural convection. ARPN J Eng Appl Sci. 2016;11(10):5.
[21] Awad OI, Mamat R, Ibrahim TK, et al. Effects of fusel oil water content reduction on fuel properties, performance and emissions of SI engine fueled with gasoline-fusel oil blends. Renewable Energy. 2018;118:858-869.
[22] Kawaguchi K, Okui K, Kashi T. The heat transfer and pressure drop characteristics of finned tube banks in forced convection (comparison of the pressure drop characteristics of spiral fins and serrated fins). Heat Transfer-Asian Res. 2004;33(7):431-444.
[23] Al-Sammarraie ATA, Jassem RR, Ibrahim TK. Mixed convection heat transfer in inclined tubes with constant heat flux. Eu J Scientific Res. 2013;97(1):144-158.
[24] Kawaguchi K, Okui K, Kashi T. Heat transfer and pressure drop characteristics of finned tube banks in forced convection (comparison of the heat transfer characteristics between spiral fin and serrated fin). Heat Transfer-Asian Res. 2005;34(2):120-133.
[25] Kawaguchi K, Okui K, Asai T, Hasegawa Y. The heat transfer and pressure drop characteristics of finned tube banks in forced convection (effects of fin height on pressure drop characteristics). Heat Transfer-Asian Res. 2006;35(3):179-193.
[26] Tahseen TA, Ishak M, Rahman M. Analysis of laminar forced convection of air for crossflow over two staggered flat tubes. Int J Automotive Mech Eng. 2012;6(1):755-767.
[27] Bahaidarah HM, Anand N, Chen H. A numerical study of fluid flow and heat transfer over a bank of flat tubes. Numerical Heat Transfer, Part A: Appl. 2005;48(4):359-385.
[28] M. Ishak, T.A. Tahseen, M.M. Rahman, Experimental investigation on heat transfer and pressure drop characteristics of air flow over a staggered flat tube bank in crossflow, Int. J. Automot. Mech. Eng. 7 (2013) 900–911.
[29] Collett, C.V. and Hope, A.D., 1983, Engineering Measurements, ELBS, Singapore.
[30] Rogers, G.F.C. and Mayhew, Y.R. 2004. Thermodynamic and transport properties of fluids. 5th ed. UK: Blackwell Publishing.
[31] Naik, S., Probert, S.D., and Shilston, M.J., 1987, "Forced-Convective Steady-State Heat Transfers from Shrouded Vertical Fin Arrays, Aligned Parallel to an Undisturbed Air-Stream," Applied Energy, 26(2), 137–158.
[32] Shah, R.K. and Sekuli'c, D.P., 2003, Fundamentals of Heat Exchanger Design, John Wiley & Sons, Inc. Hoboken, New Jersey.
[33] Figliola, R.S. and D.E. Beasley, Theory and design for mechanical measurements. 2014: John Wiley & Sons.
[34] Figliola, R.S. and D.E. Beasley, Theory and design for mechanical measurements. Measurement Science and Technology, 2001. 12(10): p. 1743-174

Table 1: Summary of the experimental uncertainty.

| Parameter | Uncertainty | |
|---|---|---|
| | Min. (%) | Max. (%) |
| $T_{in}$ | 1.23 | 1.277023 |
| $T_{\text{out}}$ | 1.164 | 1.2075694 |
| $T_w$ | 0.995 | 1.0297279 |
| $\rho_a$ | 0.2925257 | 0.303 |
| $c_{\text{pa}}$ | 0.002487 | 0.00250 |
| $\mu a$ | 0.2052682 | 0.22830 |
| $k_a$ | 0.2707462 | 0.31260 |
| $\widehat{\Delta p}$ | 1.4370612 | 1.46490 |
| Re | 3.4779685 | 3.50880 |
| $\hat{Q}$ | 3.7111928 | 3.94200 |
| Pr | 0.381 | 0.40584708 |
| Nu | 4.9842301 | 5.28200 |
| $\dot{m}$ | 3.4433808 | 3.46920 |
| $H_P$ | 3.74267058 | 3.86728715 |
| $u_{in}$ | 3.42724902 | 3.4551 |
| $T_b$ | 0.16564835 | 0.16632055 |
| Qa | 3.86599216 | 4.57660 |
| $f$ | 2.89564342 | 3.025300 |
| $h_f$ | 4.67543904 | 4.846000 |
| $ID_t$<br>$OD_t$ | ----------<br>---------- | 0.4330<br>0.4350 |
| $ID_l$<br>$OD_l$ | ----------<br>---------- | 0.2440<br>0.19970 |
| $D_h$ | 0.47172666 | 0.47540 |
| $AS_{\ O}$ | 2.22747041 | 2.3690 |
| L | ------ | 0.11240 |
| $t_{\ f}$ | ----- | 2.28800 |
| $W_x$ | ------ | 0.11324812 |
| $H_y$ | ------ | 0.11244812 |
| $E$ | 1.56102661 | 1.63910 |
| I | 3.21666501 | 3.42460 |
| $Q_{in} = I \times E$ | 3.57543534 | 3.79670 |
| $U_{\ \infty}$ | 3.42724902 | 3.52291542 |
| l | ------- | 1.88230 |
| $\theta$ | 2.2173870 | 2.42085 |
| v | 0.56947265 | 0.90950934 |
| h | 4.58206258 | 5.25130 |
| $\nu_a$ | 0.76854313 | 0.79960 |
| $\alpha_a$ | 0.42563476 | 0.43980 |
| $J$ | 3.68520831 | 3.78570 |

**Nomenclature:**

| | |
|---|---|
| D | Diameter, m |
| $D_h$ | Hydraulic diameter |
| $DT$ | Transverse Diameter, m |
| $DL$ | Longitudinal Diameter, m |
| $H$ | Domain Height, m |
| h | Convection heat transfer coefficient |
| k | Thermal Conductivity, W/m K |
| Re | Reynolds Number |
| Nu | Nusselt Number |
| P | Pressure, Pa |
| Pr | Prandtl Number |
| $SL$ | Longitudinal Pitch, mm |
| $Q_{ds}$ | Dimensionless Heat Transfer Rate |
| $P_{ds}$ | Dimensionless pressure Drop |
| $SL/DT$ | Dimensionless Longitudinal Pitch |
| ST | Transverse Pitch, mm |
| L | Length, m |
| Ld | Downstream Fin Length |
| $Lu$ | Upstream Fin Length |
| T | Temperature, °C |
| t | Fin Thickness, mm |
| u, v | Velocities in X And Y Directions, m/s |
| U, V | Dimensionless Velocities in X And Y Direction |
| x, y | Cartesian Coordinates, m |
| X, Y | Dimensionless Cartesian Coordinates |
| $\Delta p$ | Pressure drop |
| $\dot{m}$ | Mass flowrate |
| W | Width |
| $ST/DT$ | Dimensionless Transverse Pitch |
| $Lu/DT$ | Dimensionless Upstream Fin Length |